The Astrophysical Journal, 949:104 (16pp), 2023 June 1 https://doi.org/10.3847/1538-4357/acc8cc

Seven Reflares, a Mini Outburst, and an Outburst: High-amplitude Optical Variations in the Black Hole X-Ray Binary Swift J1910.2–0546

Payaswini Saikia[1], David M. Russell[1], Saarah F. Pirbhoy[1], M. C. Baglio[1,2], D. M. Bramich[1,3], Kevin Alabarta[1], Fraser Lewis[4,5], and Phil Charles[6]
[1] Center for Astro, Particle and Planetary Physics, New York University Abu Dhabi, PO Box 129188, Abu Dhabi, UAE; ps164@nyu.edu
[2] INAF, Osservatorio Astronomico di Brera, Via E. Bianchi 46, I-23807 Merate (LC), Italy
[3] Division of Engineering, New York University Abu Dhabi, PO Box 129188, Saadiyat Island, Abu Dhabi, UAE
[4] Faulkes Telescope Project, School of Physics and Astronomy, Cardiff University, The Parade, Cardiff CF24 3AA, Wales, UK
[5] Astrophysics Research Institute, Liverpool John Moores University, 146 Brownlow Hill, Liverpool L3 5RF, UK
[6] Department of Physics & Astronomy, University of Southampton, Southampton SO17 1BJ, UK
Received 2022 November 15; revised 2023 March 20; accepted 2023 March 28; published 2023 June 2

Abstract

We present long-term (2012–2022) optical monitoring of the candidate black hole X-ray binary Swift J1910.2–0546 with the Faulkes Telescopes and Las Cumbres Observatory network. Following its initial bright 2012 outburst, we find that the source displayed a series of at least seven quasi-periodic, high-amplitude (~3 mag) optical reflares in 2013, with a recurrence time increasing from ∼42 to ∼49 days. In 2014, the source experienced a mini outburst with two peaks in the optical. We also study the recent 2022 outburst of the source at optical wavelengths, and perform a comparative analysis with the earlier rebrightenings. A single X-ray detection and only two radio detections were obtained during the 2013 reflaring period, and only optical detections were acquired in 2014. During the reflaring in both 2013 and 2014, the source showed bluer-when-brighter behavior, having optical colors consistent with blackbody heating and cooling between 4500 and 9500 K, i.e., the temperature range in which hydrogen starts to ionize. Finally, we compare the flaring behavior of the source to rebrightening events in other X-ray binaries. We show that the repeated reflarings of Swift J1910.2–0546 are highly unusual, and propose that they arise from a sequence of repetitive heating and cooling front reflections traveling through the accretion disk.

Unified Astronomy Thesaurus concepts: Stellar mass black holes (1611); Low-mass x-ray binary stars (939); Accretion (14); Jets (870); Optical astronomy (1776)

1. Introduction

Low-mass X-ray binaries (LMXBs) are systems in which a low-mass ($M < M_{\odot}$) companion star is orbiting a compact object, either a neutron star (NS) or a black hole (BH). The companion (main sequence or evolved) star fills its Roche lobe and transfers mass toward the compact object, forming an accretion disk around it. When this accretion disk becomes unstable, the inflowing matter in the disk heats up, becomes ionized, and this initiates an outburst, in which the optical and X-ray luminosity can increase by several orders of magnitude (e.g., Dubus et al. 2001; Lasota 2001). LMXBs emit most of their power in the X-ray band by releasing the gravitational potential energy of the accreted matter. Often during an outburst, collimated synchrotron-emitting compact jets are launched (e.g., Corbel et al. 2000; Fender 2004), analogous to the jets observed in supermassive BHs hosted by active galactic nuclei (e.g., Blandford & Königl 1979). Accreting BHs, spanning several orders of magnitude in BH mass, follow a correlation between the X-ray and radio luminosity normalized by mass, indicating coupling between the jet and the inflowing matter (e.g., Merloni et al. 2003; Falcke et al. 2004; Saikia et al. 2015, 2018).

Outbursts of BH X-ray binaries (BHXBs) typically last months to years and are quite often characterized by a fast-rise, exponential-decay light-curve profile (e.g., Chen et al. 1997; Tetarenko et al. 2016, and references therein). However, there are many exceptions, with some sources rising slowly, some having multiple peaks, and some displaying flares, dips, plateaus and rebrightenings (e.g., Buxton et al. 2012; Kalemci et al. 2013; Zhang et al. 2019, and references therein). While reflares during outburst decays are fairly common, rebrightenings after the outburst's end, when the source has reached quiescence, have been reported in far fewer sources. These rebrightenings usually peak at a fainter luminosity than the first outburst and last a shorter time; such events are coined mini outbursts (see Zhang et al. 2019, for classifications of rebrightening events in LMXBs). The origin of reflares, and mini outbursts in particular, are a matter of debate. X-rays from the main outburst heat the companion star, which could increase mass transfer into the disk, causing outburst "echoes" (e.g., Dubus et al. 2001; Kalemci et al. 2014). Sometimes these reflares can also be observed in the optical and infrared (e.g., Zhang et al. 2019), and they can also be caused by the reactivation of jets during outburst decays (e.g., Jain et al. 2001; Kalemci et al. 2013; Russell et al. 2020). In NS LMXBs, multiple flares (at different timescales) could be caused by the propeller effect, which has been proposed to change the mass accretion rate due to the rapidly rotating NS magnetosphere (Hartman et al. 2011; Patruno et al. 2016).

Historically, many mini outbursts and late rebrightening events may have been missed, due to their faintness and a lack of either sensitive X-ray telescopes or regular optical monitoring. Long-term optical monitoring of LMXBs, in particular

using robotic telescopes, provides an inexpensive way to monitor their activity at low accretion rates, even for long periods of quiescence. Several LMXB outbursts and rebrightening events have been identified using this method (e.g., Callanan et al. 1995; Corral-Santana et al. 2010b; Lewis et al. 2010; MacDonald et al. 2014), especially more recently (e.g., Russell et al. 2018; Zhang et al. 2019; Goodwin et al. 2020; Pirbhoy et al. 2020; Saikia et al. 2021; Alnaqbi et al. 2022; Baglio et al. 2022). Optical transient surveys have also detected some LMXB brightenings in recent years (e.g., Drake et al. 2017; Tucker et al. 2018; van Velzen et al. 2019).

1.1. Swift J1910.2–0546

Swift J1910.2–0546 (MAXI J1910−057, hereafter J1910.2) was independently discovered by the Neil Gehrels Swift Observatory (Swift; Burrows et al. 2005) and the Monitor of All-sky X-ray Image (MAXI; Matsuoka et al. 2009), when the source went into an outburst in 2012 May (Krimm et al. 2012a; Usui et al. 2012). The 2012 outburst was extensively studied using X-ray spectral and timing analysis (e.g., Degenaar et al. 2014; Nakahira et al. 2014), optical photometry (Saikia et al. 2023) and spectroscopy (Casares et al. 2012; Charles et al. 2012). From these detailed studies, J1910.2 was was found to be a likely BH candidate at a distance of $d > 1.7$ kpc (Nakahira et al. 2014). Optical variability of the source suggests the orbital period to be fairly short (∼2–4 hr; Lloyd et al. 2012) with an upper limit of $\leqslant$6 hr (Saikia et al. 2023), although we note that a larger value is expected from spectroscopic studies ($\geqslant$6.2 hr; Casares et al. 2012).

Following the 2012 outburst, Swift and MAXI continued to detect J1910.2 until 2013 January, after which the flux levels of the source had decreased below the detection limits. Radio detections were obtained on 2013 March 9 and May 3, along with Swift observations on March 9 (optical detection, X-ray nondetection) and May 10 (X-ray detection; Tomsick et al. 2013). No further observations of J1910.2 have been reported since 2013 May, except optical (2015 July) and near-infrared (NIR; 2017 April) detections in quiescence (López et al. 2019), until the recent enhancement of activity of the source in 2022. A new X-ray outburst from J1910.2 was detected in 2022 February (Tominaga et al. 2022), when it was also found to be prominent in the radio (Williams et al. 2022) and optical (Hosokawa et al. 2022; Kong 2022). The source quickly and steadily decayed at all wavelengths, and was found to be back in optical quiescence by the end of 2022 March (Saikia et al. 2022a).

Here we report the long-term optical monitoring of J1910.2 with the Faulkes Telescopes[7] and Las Cumbres Observatory (LCO)[8] network of telescopes from 2012 to 2022. We mainly focus on two periods of activity that were previously undocumented—a series of strong flaring in 2013, and a faint mini outburst in 2014. We combine our optical data with Swift and MAXI monitoring (at UV and X-ray wavelengths) and radio data from the literature to discuss the optical emission processes in J1910.2 throughout quiescence and outbursts, and explore the various physical explanations behind the flaring activity and the mini outburst. The observations are described in Section 2, and the results are presented and discussed in Section 3. We include a comparative analysis of the reflares with other BHXB systems in Section 4, and a summary is provided in Section 5.

2. Observations

2.1. Faulkes Telescope/LCO Monitoring

We have been monitoring J1910.2 at optical wavelengths since its discovery in 2012, using the 2 m Faulkes Telescopes at Haleakala Observatory (Maui, Hawai"i, USA) and Siding Spring Observatory (Australia), as well as the 1 m telescopes at Siding Spring Observatory (Australia), Cerro Tololo Inter-American Observatory (Chile), McDonald Observatory (Texas), Teide Observatory (Tenerife), and the South African Astronomical Observatory (SAAO, South Africa) of the LCO network (Brown et al. 2013). The observations were performed in the Bessell B, V, R and Sloan Digital Sky Survey (SDSS) i' filters, as part of an ongoing monitoring campaign of ∼50 LMXBs (Lewis et al. 2008). We use the "X-ray Binary New Early Warning System (XB-NEWS)" data analysis pipeline (Russell et al. 2019; Goodwin et al. 2020; Pirbhoy et al. 2020) for calibrating the data and performing aperture photometry (see Saikia et al. 2023, for more details). This process resulted in photometric measurements of J1910.2 in a total of 123 (B), 74 (V), 85 (R), and 211 (i') images (see Tables A1–A4) between 2012 June 14 (MJD 56092) and 2022 March 20 (MJD 59658).

We note that J1910.2 lies in the Galactic plane, with a few faint stars within 2″ of the source position (López et al. 2019). These stars may contribute to the quiescent flux measurements, but are too faint to affect the active interval photometry. Due to the limitation in the resolution and sensitivity of the Faulkes and LCO Telescopes, it is difficult to provide a proper numerical estimate of the contribution of the two neighboring stars to the quiescent magnitude of the source.

2.2. Archival X-Ray and UV Monitoring

We acquired the X-ray detections of J1910.2 obtained with the X-Ray Telescope (XRT; Burrows et al. 2005) onboard Swift, using the online Swift/XRT data products generator[9] maintained by the Swift data center at the University of Leicester (see Evans et al. 2007; Evans et al. 2009). The source was observed for 67 days during its 2012 outburst (see Saikia et al. 2023) in the Windowed Timing (WT) mode (Hill et al. 2004). Due to Sun constraints, no observations were taken by Swift/XRT from 2012 November until 2013 March. It was again observed in Photon Counting (PC) mode (Hill et al. 2004) for five days between 2013 March to September, with exposures ranging from ∼1000 to ∼2000 s (Observation ID 00032742), and was detected only once (see Table A5). In addition to the Swift/XRT light curve, we also acquired the 2–10 keV MAXI/GSC light curve.[10] Unfortunately, during the flaring activity of J1910.2, MAXI only detected the system once above 3σ significance.

We also retrieved the publicly available Swift Ultraviolet and Optical Telescope (UVOT; Roming et al. 2005) observations from the NASA/HEASARC data center. We use the pipeline processed images and follow the `uvotsource` HEASOFT routine to obtain the magnitudes of the source using an aperture size of 5″ centered on the source. During the 2012 outburst, the

[7] http://www.faulkes-telescope.com/
[8] https://lco.global/
[9] https://www.swift.ac.uk/userobjects/
[10] http://maxi.riken.jp/top/index.html

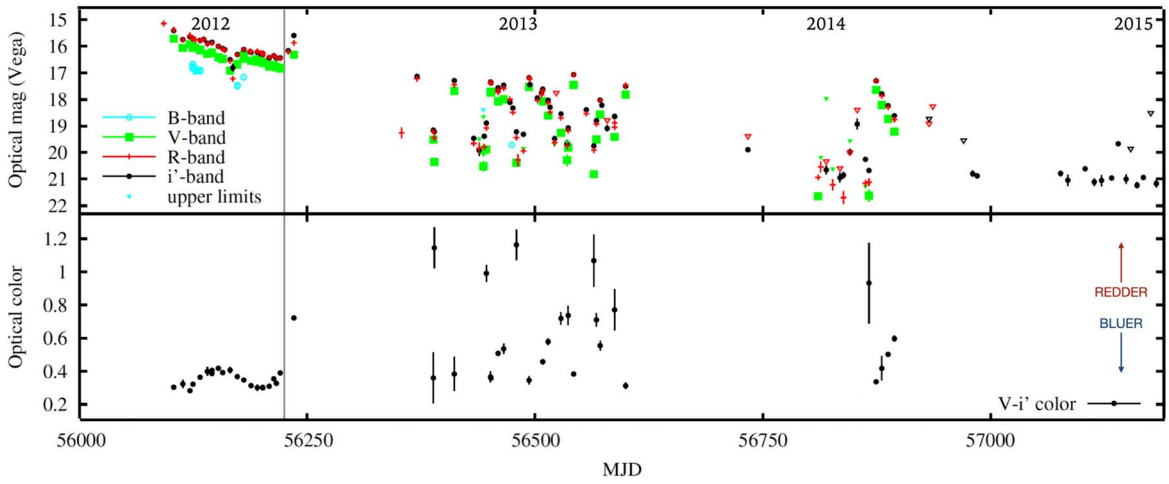

Figure 1. Long-term light curve (top; in B, V, R, and i') and color (bottom; $V - i'$) of J1910.2 from 2012 to 2015. The gray vertical line (at MJD 56225) shows the transition to a pure hard state during the 2012 outburst.

source was detected in almost all the epochs observed by Swift/UVOT, for a varying range of exposures between ∼20 and 1000 s (see Saikia et al. 2023). However, most of the observations during the flaring period and the faint mini outburst during 2013 and 2014 were nondetections (the significance of the detection above the sky background is lower than 5σ, see Table A5), despite having much longer exposure times (even for ∼1000 s exposures).

2.3. Radio Data

We searched the literature for detections of J1910.2 after the 2012 outburst. In 2013, detections were acquired by the Australia Telescope Compact Array (ATCA) in March and May at 5.5 and 9 GHz on both dates, with average flux densities of 0.06 mJy in March and 0.3–0.4 mJy in May (no errors are given; Tomsick et al. 2013). It was again detected during its 2022 outburst with the Arcminute Microkelvin Imager Large Array (AMI-LA; Zwart et al. 2008; Hickish et al. 2018) at 15.5 GHz (Williams et al. 2022).

3. Results and Discussion

In Figure 1 we present the long-term LCO optical data of J1910.2 in B, V, R, and i' as well as the $V - i'$ color, from the start of the 2012 outburst until 2015. After the main 2012 outburst there is a gap (Sun constraint), following which, in 2013, J1910.2 was found to be undergoing high-amplitude flaring (see Section 3.1). In 2014 there was a short mini outburst (Section 3.2) followed by quiescence. The color variability (Figure 1) shows that, during the reflares and mini outburst, the source follows a bluer-when-brighter behavior.

Since 2015 the source has remained in quiescence, as far as our monitoring can tell, until 2022 February, when it was observed to undergo a new outburst (see Section 3.4). Table 1 summarizes these periods of optical activity in J1910.2 during 2012–2022.

3.1. The 2013 Reflares

From MAXI and Swift X-ray data, Nakahira et al. (2014) report that the 2012 outburst of J1910.2 ended around 2013 January 26 (MJD 56318). Due to Sun constraints we have no optical coverage during the 2012 outburst decay, and when monitoring was resumed in 2013 March we found J1910.2 in a flaring state. It displayed at least seven, high-amplitude (∼3 mag), quasi-periodic optical reflares (with the interval between reflares increasing from ∼42 to ∼49 days), which continued for at least eight months. Due to the lack of coverage before 2013 March, it is not evident if and when the source entered quiescence before the rebrightening, and it is also not possible to constrain the exact date when the reflaring started or ended.

Table 1
Summary of Optical Periods of Activity in J1910.2 during 2012–2022

Activity[a]	Year	N_{fl}[b]	Peak i'(mag)
Outburst	2012 May–2013 Jan	1	15.41 ± 0.01
Reflares	2013 Feb–Nov	⩾7	∼17.0–17.5
Mini outburst	2014 Jun–Sep	2	17.30 ± 0.01
Outburst	2022 Feb–Mar	1	16.45 ± 0.01

Notes.
[a] Rebrightening classification based on Zhang et al. (2019).
[b] Number of flares seen during the period of rebrightening.

We plot the 2013 rebrightening activities of the source in Figure 2. During the interval of 2013 February 27 to November 4 (MJD 56350 to MJD 56600), the source had unusually extreme reflares in all optical bands, which had not been seen before. The optical magnitude during the peak of these reflares reached $i' \sim$ 17–17.5. Between any two consecutive flares, the magnitudes did not drop to the quiescent value, and remained around $i' \sim$ 19–20. For a rough comparison, J1910.2 is found to have a quiescent i' of 22.18 ± 0.04 using the William Herschel Telescope with the auxiliary port camera (ACAM; 2015 July 19; López et al. 2019). The optical color ($V - i'$) roughly decreased during the rise of the flare, following a bluer-when-brighter behavior (see Figures 2(c) and 7). It was seen to be the lowest during the peak of the flares, and the color reddened during the decay of the flares. Radio and X-ray observations carried out in this period with ATCA (2013 March 9 and May 3) and Swift/XRT (2013 March 9 and May 10) show that the source was probably flaring in these bands as well (Tomsick et al. 2013). While in 2013 March, the authors report a radio flux of 0.06 mJy, it increased to 0.3–0.4 mJy in 2013 May. On the other hand, the source was not detected above 3σ significance with Swift/XRT (0.6–10 keV) during the 2013

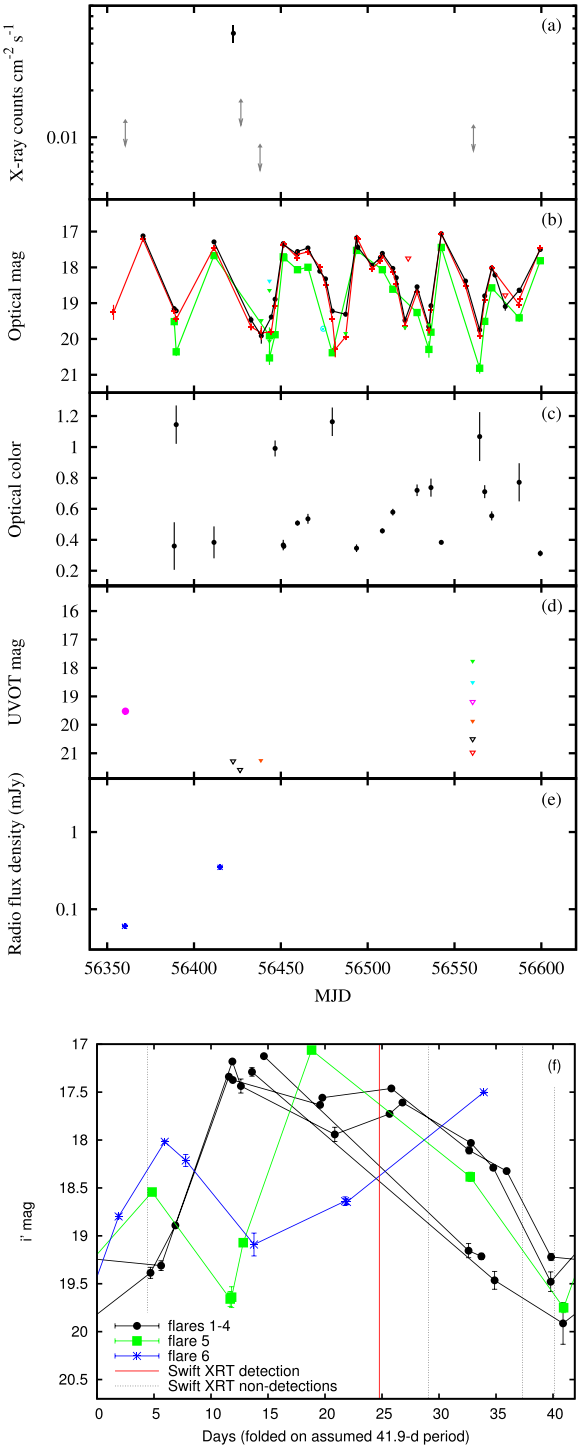

Figure 2. Upper box: flaring behavior of J1910.2 during the 2013 reflares (see Section 3.1). (a) Swift/XRT light curve. (b) Optical magnitudes in V (green squares), R (red plus), B (blue circles), and i' (black dots), with upper limits shown as inverted triangles. (c) Optical color ($V - i'$). (d) Swift UVOT magnitudes in u (magenta circles) and upper limits shown as inverted triangles in v (green), b (cyan), u (magenta), $uvw1$ (orange), $uvw2$ (red), and $uvm2$ (black). (e) Radio flux density (mJy). Lower box: (f) 2013 reflares folded on $P = 41.9$ days (the interval between the fast rises of flares 3 and 4).

March observation, but it was observed to be brighter in 2013 May (see Table A5). Inspecting the MAXI light curves in the energy band 2.0–10.0 keV for the same period, we found that J1910.2 was only detected once (MJD 56451) above 3σ significance. Taking into account the Swift/XRT and MAXI

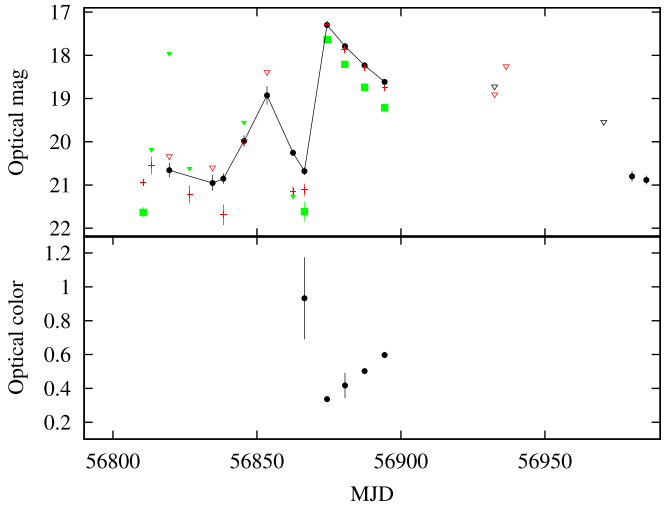

Figure 3. 2014 mini outburst of J1910.2. Upper panel: optical light curve in V (green squares), R (red plus), and i' (black circles), and upper limits as inverted triangles. The i' points are joined up to show their evolution. Bottom: optical color ($V - i'$) evolution.

detections, we estimate lower and upper limits for the X-ray flux in the energy band 2.0–10.0 keV of $\sim 4.0 \times 10^{-12}$ erg cm^{-2} s^{-1} and $\sim 3.0 \times 10^{-10}$ erg cm^{-2} s^{-1}, respectively.

The average optical cycle time of the reflares increases with time from ~42 to ~49 days. In Figure 2(f) we show the first six reflares folded on a period of 41.9 days (the time between the fast rises of flares 3 and 4). As evident from the figure, the four initial reflares have a very similar duration consistent with ~41.9 days. The first two reflares (flares 1 and 2) have a fairly sharp peak before decaying, with comparable rise and decay times. The next two (flares 3 and 4) have a rise time similar to the previous ones, but show an extended peak lasting ~15 days, before the decay. For these first four reflares, the rise time from the minimum to the peak of the reflare is ~6 days. The last two flares (flares 5 and 6) have a double-peaked morphology, with the first peak being faint and the second peak being a similar magnitude to the first four flares, and a slightly longer period (seen in Figure 2(f) as a delay in the bright peak for these flares). Multiple reflares displaying such periodic behavior have been previously observed in many dwarf novae (DNe; see, e.g., Kato 2015), but they are rarely seen in LMXBs (see Section 4 for a detailed discussion).

3.2. The 2014 Mini Outburst

When optical monitoring of J1910.2 was resumed in 2014, the source was found in a variable state close to quiescence ($i' \sim$ 20.7–21.7, see Section 3.6). Shortly thereafter, the source became brighter again (see Figure 3), showing two consecutive peaks on MJD 56853.5 ($i' = 18.93 \pm 0.21$) and a brighter one on MJD 56874.3 ($i' = 17.30 \pm 0.01$). There was a single LCO detection of the source between the 2013 reflares and the 2014 rebrightening (2014 March 17, MJD 56733.6, $i' = 19.89 \pm 0.09$), which is much fainter than the reflares, but brighter than the typical quiescence value obtained with LCO ($i' \sim$ 20.7–21.7, see Section 3.6). Due to the lack of continuous observations during that period, it cannot be confirmed if the 2013 reflares were going on for the whole year and the rebrightening events seen in 2014 were just a continuation of the 2013 reflares.

The peak of the 2014 rebrightening on May 8 (MJD 56874.3, $i' = 17.30 \pm 0.01$) is almost ∼2 mags fainter than the 2012 outburst peak on MJD 56103.6 ($i' = 15.41 \pm 0.01$). Although comparable to the peak magnitudes observed during the 2013 reflares (i'-band range ∼17.0–17.5, see Table 1), we classify the 2014 rebrightening as a mini outburst because the source had reached close to quiescence before the apparent brightening. Moreover, it follows a typical double-peaked outburst profile with a sudden rise from quiescence followed by an exponential decay after the second peak. The evolution of the optical color ($V - i'$) during the mini outburst also follows a bluer-when-brighter behavior, similar to the 2013 reflares. This is clearly observed during the second peak of the mini outburst, where the source is bluest at the peak, and slowly reddens as it decays during the return of the mini outburst to quiescence.

3.3. The 2022 Outburst

Recently, renewed X-ray activity was detected in J1910.2 by MAXI/GSC on 2022 February 4 (MJD 59614), with the 2–6 keV flux reaching 17 mCrab on February 5 (MJD 59615), and then gradually declining to ∼7 mCrab on February 7 (MJD 59617; Tominaga et al. 2022). The source quickly faded below the detection limit in soft X-rays, and returned to close to quiescence (see Figure 4(d)). It was detected in the radio by AMI-LA (Hickish et al. 2018; Zwart et al. 2008) at 15.5 GHz, with integrated fluxes of 4.1 ± 0.6 mJy on 2022 February 7 (MJD 59617.377), 7.0 ± 0.8 mJy on February 9 (MJD 59619.411), and 9.0 ± 1.0 mJy on February 10 (MJD 59620.376), indicating that the source was rapidly brightening (see Figure 4(c); values obtained from Williams et al. 2022).

LCO first detected J1910.2 during the recent activity on 2022 February 13 (MJD 59623.27), after the source came out of a Sun constraint (see Figure 4(a)). At that time, it was already at peak, or at an early decline stage of the outburst (with $i' \sim 16.45 \pm 0.01$). This is brighter than the previous rebrightening events of 2013 (flares with peaks in the range of $i' \sim 17.0$–17.5 mag,) and the mini outburst of 2014 ($i' \sim 17.30 \pm 0.01$), and fainter than the previous 2012 outburst with $i' \sim 15.41 \pm 0.01$ on 2012 June 25 (MJD 56103.6, see Table 1). An optical nondetection was reported on 2022 February 8 (MJD 59618.85) with the MITSuME 50 cm telescope Akeno, implying 5σ upper limits of $R_c > 17.0$ and $I_c > 16.6$, before brightening and being detected on 2022 February 15 (MJD 59625.84) with $R_c = 16.9 \pm 0.1$ and $I_c = 16.7 \pm 0.1$ (Hosokawa et al. 2022). It was also detected by the Zwicky Transient Facility (ZTF; Bellm et al. 2019) on 2022 February 11 (MJD 59621) with $r \sim 16.4$, which got gradually fainter with $r \sim 16.6$ on February 12 (MJD 59622) and $r \sim 17.2$ on February 18 (MJD 59628; Kong 2022). Following the rebrightening classification scheme based on Zhang et al. (2019), we classify the recent activity as a new outburst, as the flux reached quiescence before the rebrightening event, and the time separating the start of the quiescent period (after the end of the last activity) from the start of the recent rebrightening is much larger than the duration of the outburst.

3.4. Spectral Energy Distributions

We build the dereddened spectra and spectral energy distributions (SEDs) of J1910.2 using quasi-simultaneous observations (within 24 hr) both in quiescence (see Figure 5),

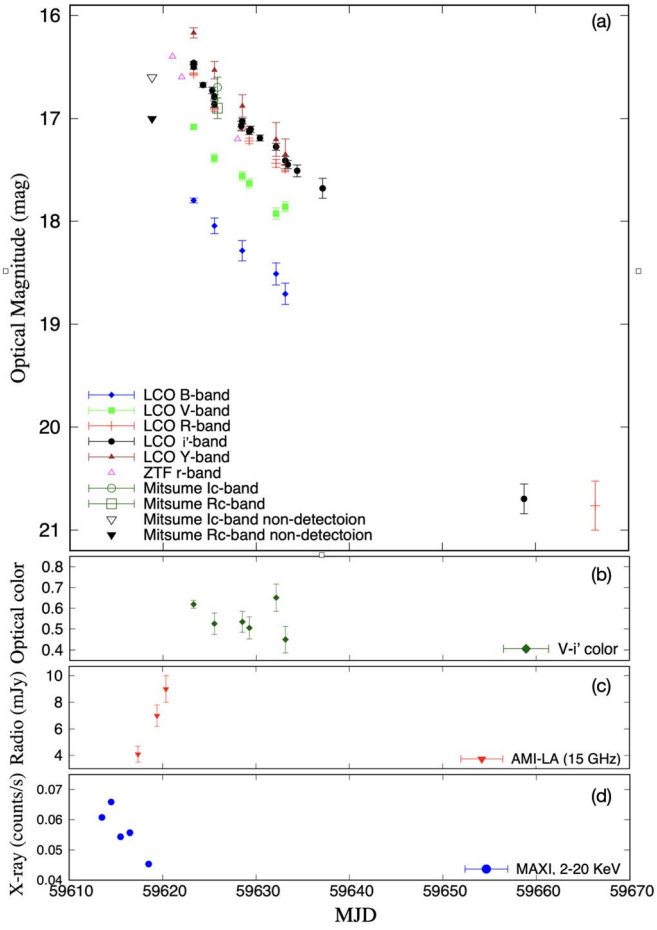

Figure 4. 2022 outburst of J1910.2. (a) Optical light curves in B (blue, filled diamonds), V (green, filled squares), R (red, plus), i' (black circles), and Y (brown, triangles), and upper limits as inverted triangles. Also plotted are the available data in the literature from the MITSuME telescope, including nondetections (inverted triangles; Hosokawa et al. 2022), and the ZTF telescope (magenta, open triangles; Kong 2022). (b) Optical color ($V - i'$) evolution. (c) Radio flux density (in mJy) obtained with the AMI-LA telescope at 15 GHz (Williams et al. 2022). (d) MAXI 2–20 keV daily average light curve (for data with $\geqslant 4\sigma$ significance).

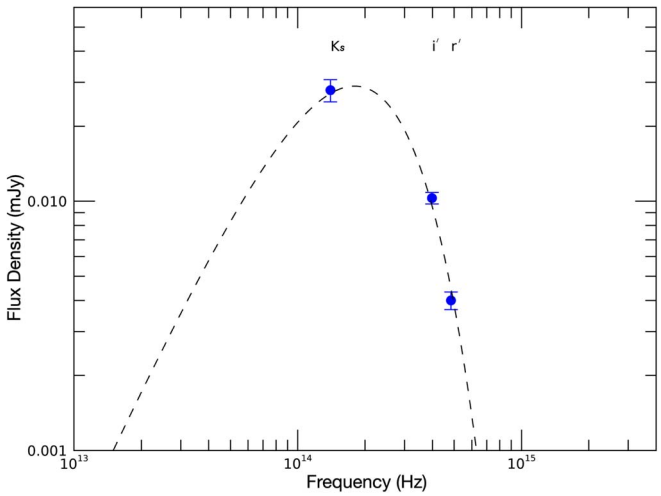

Figure 5. Single temperature blackbody fit to the intrinsic (dereddened) IR/optical SED during quiescence, with optical fluxes obtained from López et al. (2019).

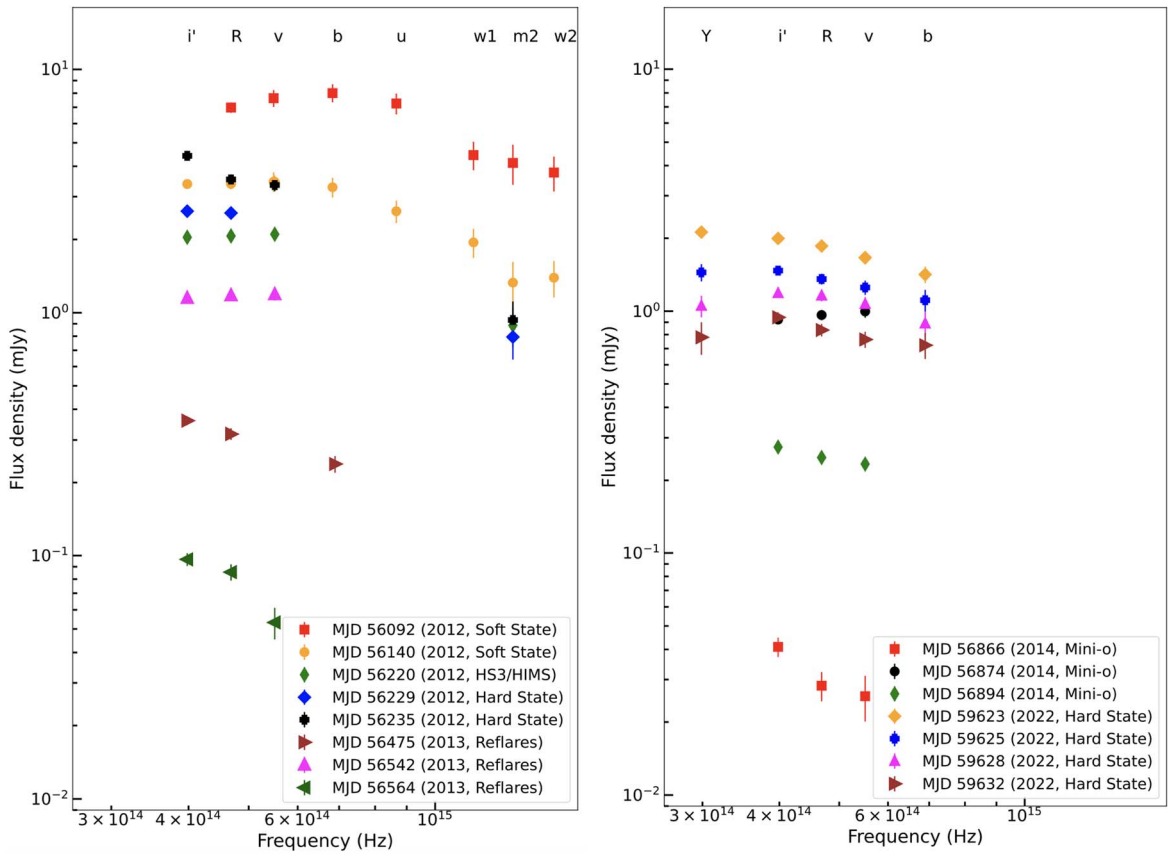

Figure 6. Intrinsic (dereddened) optical/UV SEDs of J1910.2 with quasi-simultaneous data (taken within 24 hr) during the 2012 and 2022 outbursts, as well as the 2013 reflares, and the 2014 mini outburst.

and in the bright episodes of the 2013 reflares, the 2014 mini outburst, and the 2022 outburst (see Figure 6). We also overplot a few SEDs from different spectral states of its discovery outburst in 2012 for comparison (see Saikia et al. 2023, for the evolution and the naming of the spectral states in J1910.2). Dereddened fluxes were obtained from the calibrated magnitudes using a hydrogen column density value of $N_{\rm H} = (3.5 \pm 0.1) \times 10^{21}$ cm^{-2} (Degenaar et al. 2014) and the Foight et al. (2016) and Cardelli et al. (1989) extinction laws to estimate the absorption coefficients (see Table 1 in Saikia et al. 2023, for more details).

For J1910.2, a simple fitting of the quiescent spectra (using values obtained from López et al. 2019) with a single-temperature blackbody gives a value of ∼3040 K (Figure 5). Assuming that there is no accretion activity at these lowest fluxes, then this temperature is consistent with an M4-type star, of mass $\sim 0.3\,M_{\odot}$ and radius $\sim 0.3\,R_{\odot}$ (see Saikia et al. 2023).

During the outbursts and rebrightening episodes, the optical/UV spectra are found to be fairly smooth. For the brighter outburst epochs, we find a slightly positive to flat slope in the optical ($\alpha_{R-b} = -0.04$–0.35, where $F_{\nu} \propto \nu^{\alpha}$), and a negative slope in the UV ($\alpha_{u-w2} = -1.0$ to -1.2, see Figure 6). The SEDs peak around V or B for the brighter epochs of the 2012 outburst, but appear redder (around i') for the 2022 outburst. During the rebrightening epochs of the 2013 reflares and 2014 mini outburst, the i' flux is generally found to be brighter than the higher frequencies, unlike the brighter epochs of the 2012 outburst (see Table 2 for a comparison of the optical spectral indices). This could be a hint of the blackbody peak shifting to lower frequencies, as the luminosity decreases. The overall shapes of the optical/UV spectra are consistent with the outer regions of a blue, X-ray irradiated accretion disk (e.g., Hynes 2005).

Table 2
List of Optical Spectral Indices for the Spectra Presented in Figure 6

Year	MJD	State	Spectral Index
2012	56092	Soft	$\alpha_{R-b} = 0.35 \pm 0.09$
2012	56140	Soft	$\alpha_{i'-b} = -0.04 \pm 0.06$
2012	56220	HS3/HIMS	$\alpha_{i'-v} = 0.09 \pm 0.01$
2012	56229	Hard	$\alpha_{i'-R} \sim -0.11$[a]
2012	56235	Hard	$\alpha_{i'-v} = -0.85 \pm 0.30$
2013	56475	Reflares	$\alpha_{i'-b} = -0.74 \pm 0.01$
2013	56542	Reflares	$\alpha_{i'-v} = 0.11 \pm 0.03$
2013	56564	Reflares	$\alpha_{i'-v} = -1.83 \pm 0.63$
2014	56866	Mini outburst	$\alpha_{i'-v} = -1.45 \pm 0.48$
2014	56874	Mini outburst	$\alpha_{i'-v} = 0.24 \pm 0.02$
2014	56894	Mini outburst	$\alpha_{i'-v} = -0.50 \pm 0.07$
2022	59623	Hard	$\alpha_{i'-b} = -0.38 \pm 0.08$
2022	59625	Hard	$\alpha_{i'-b} = -0.23 \pm 0.11$
2022	59628	Hard	$\alpha_{i'-b} = 0.05 \pm 0.16$
2022	59632	Hard	$\alpha_{i'-b} = -0.04 \pm 0.26$

Note. $\alpha_{i'-b}$ is shown unless otherwise specified.
[a] As only two data points are available, we are unable to calculate the uncertainty.

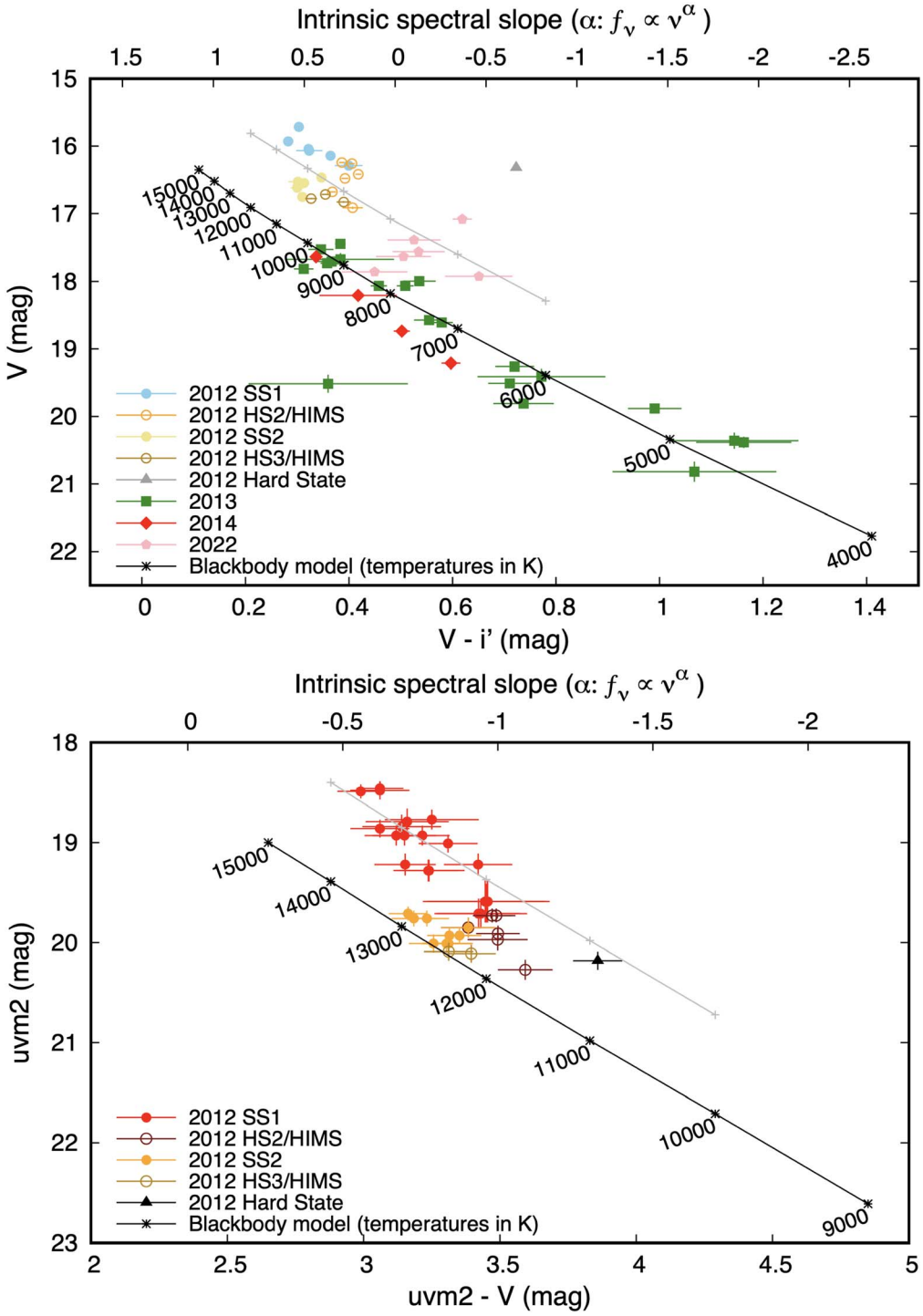

Figure 7. CMDs of J1910.2 in (upper) V vs. $V - i'$, and (lower) $uvm2$ vs. $uvm2 - V$. The black solid lines show points from single-temperature blackbody models heating up and cooling (with the normalization fixed according to the trend in the V vs. $V - i'$ CMD for both plots). The gray lines show a different normalization to better fit only the 2012 outburst.

3.5. Color Evolution

In order to analyze the color evolution of J1910.2, we plot the optical color–magnitude diagram (CMD) using quasi-simultaneous V-band and i'-band magnitudes (Figure 7, top panel), and the optical/UV CMD using $uvm2$-band and V-band magnitudes (Figure 7, bottom panel). The different states of the 2012 outburst, the subsequent rebrightening events, and the 2022 outburst are shown in different colors and symbols to distinguish their temperature ranges and study their comparative behaviors. We also plot the single temperature blackbody model of Maitra & Bailyn (2008), which approximates the emission of an X-ray irradiated outer accretion disk (see also Russell et al. 2011; Zhang et al. 2019; Baglio et al. 2020b, 2022; Saikia et al. 2022c). The normalization of the blackbody model depends on various factors, including the accretion disk radius, which can be estimated from the system masses, orbital period, inclination, source distance, disk filling

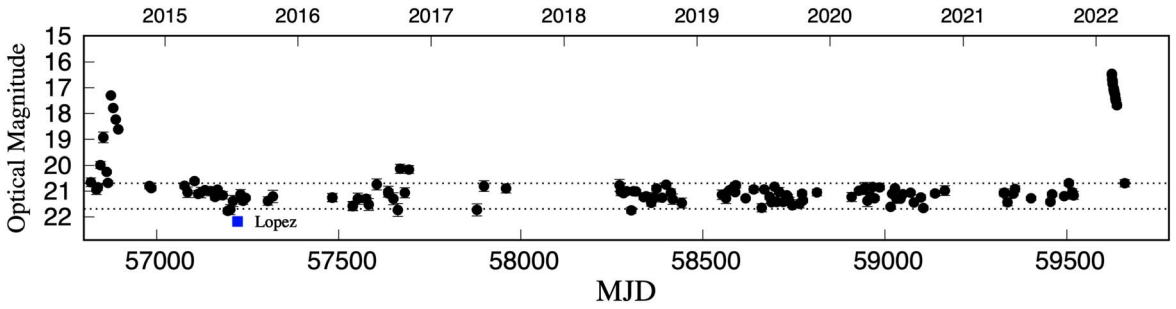

Figure 8. Long-term (2014–2022) i' light curve of J1910.2 from LCO. The dotted horizontal lines indicate the typical range of quiescence ($i' \sim$ 20.7–21.7), although it should be noted that they could be contaminated by a few faint, nearby stars (see text). For comparison, we plot (in blue square) the WHT+ACAM quiescent photometry of López et al. (2019).

factor, disk warping, etc. As many of these parameters are poorly constrained, we fix the normalization value to what best describes the trend in the optical CMD as it has the most amount of data. Among the observations, we optimize the normalization so as to cover the widest range of observed optical color ($V - i'$). We use the same normalization also for the optical/UV CMD.

We find that the observations taken during the reflares in 2013 and the mini outburst in 2014 are well represented by the disk model (shown as a solid black line in Figure 7). During these rebrightening events, the outer disk temperature is approximately between 4500 and 9500 K. This covers the expected temperature range where hydrogen in the disk gets ionized (∼7000–10,000 K). We find that the disk temperature during these rebrightening events repeatedly increases and then decreases, suggesting that the reflares are caused by continuous waves of heating and cooling flowing through the accretion disk.

However, the initial outburst of 2012 does not completely follow the same model of single-temperature blackbody heating and cooling. The temperature during this main outburst is higher than the H ionization temperature (∼11,000 K), and the emission is redder and/or brighter than what is expected from the disk model. We find that the data are better represented by a single-temperature blackbody model with a different normalization (shown as a solid gray line in Figure 7). This could either be due to significant contribution to the optical emission from additional components such as synchrotron emission from a jet, or because the viscous disk starts to dominate, or else because of disk warping. The factor difference between the two normalizations is 2.75 in flux, indicating the expected increase in the surface area needed to explain the brighter points from the initial outburst, compared to the reflares and mini outburst.

We note that synchrotron emission is unlikely to be the dominant cause, as the brighter and redder trend is also observed in the soft state, when we do not expect the jet to be present. Jets have been observed in the IR/optical during transition from the soft state to the soft-intermediate state (e.g., Russell et al. 2020), but for a prolonged time, and not in the soft state. The observations taken during the 2012 outburst in the pure hard state are much redder compared to all the other data points, especially in the optical CMD representing longer wavelengths (V versus $V - i'$), which trace the highest jet contribution. In this case, the significant deviation of the data points away from the disk model can be confidently attributed to a jet, as it starts to dominate the optical emission during the transition to the pure hard state.

Even for the optical/UV CMD, where we plot the bluer wavelengths ($uvm2$ versus $uvm2 - V$) that are generally dominated by the disk with a negligible jet contribution, we find that the data in the soft as well as the hard–intermediate state (HIMS) and hard state diverged from the disk model. This suggests that the deviation of the 2012 data from the blackbody model is not because of a jet contribution, but probably has its origin in the disk.

The 2022 data are also comparatively brighter and/or redder than the disk model. As these data points are taken during the hard state, and the spectral index is too low for a viscous disk, we attribute this deviation to a jet contribution, just as in the case of the pure hard-state data of the 2012 outburst. This is also supported by the AMI-LA radio detections, which showed a considerable rise just before the LCO observations were taken (Williams et al. 2022).

3.6. Variability in Quiescence

After the end of the mini outburst in 2014, we continued the LCO monitoring of J1910.2. In Figure 8, we plot the long-term (2014–2022) optical (i') light curve of J1910.2, and find that it remained in quiescence throughout this interval, but was variable over a range of i' band ∼ 20.7–21.7. However, we do note that, during quiescence, the LCO magnitudes (mostly with forced multiaperture photometry by XB-NEWS at the source position; Goodwin et al. 2020) include some contaminating flux from two nearby stars (within 2″ of the source position), with similar brightnesses as J1910.2.

López et al. (2019) detected J1910.2 at $i' = 22.18 \pm 0.04$ on 2015 July 19 (MJD 57222) using the William Herschel Telescope with ACAM. This is the only other published quiescent magnitude of the source at optical wavelengths, in which the magnitudes obtained are not contaminated by neighboring stars. From the finding chart of López et al. (2019), we know that the two neighboring stars have brightnesses comparable to J1910.2. Assuming that the ACAM magnitudes are representative of the average magnitude of J1910.2 in quiescence, and that the two neighboring stars are of the same magnitude, we speculate that having all three stars in the same aperture (as should be the case for LCO data) would give us a flux which is thrice the real flux. This translates to an optical magnitude of $i' \sim 21.01 \pm 0.10$. In fact, we find that the average quiescent LCO mags is comparable to this, with $i' = 21.16 \pm 0.29$. As we do not have an LCO detection of the source on the same date, a direct comparison of the magnitudes is not possible, but the closest observation with LCO (MJD 57230) is also ∼1 mag brighter. As shown in Figure 8, the long-term LCO light curve suggests accretion variability in quiescence with a range of quiescent magnitudes that are ∼0.4 to ∼2.0 mag brighter in LCO compared to the López et al. (2019) value

(a range that could either be due to varying seeing conditions and/or due to intrinsic accretion variability). As the amount of flux in the blend depends on the seeing conditions, we cannot completely trust the variability observed. However, we note that although some quiescent variability is expected due to fluctuating seeing, we cannot rule out intrinsic variability, as is seen in many other BHXBs (e.g., Koljonen et al. 2016; Wu et al. 2016; Russell et al. 2018).

4. Interpretation of the Reflares

In many BHXBs, weaker secondary rebrightening events after the source has reached quiescence, either in the form of reflares or mini outbursts, follow the initial outburst (e.g., Chen et al. 1997; Tomsick et al. 2003; Muñoz-Darias et al. 2017; Cuneo et al. 2020). Such rebrightenings are also observed in NS X-ray binaries (NSXBs) and DNe. This suggests that the cause of at least some postoutburst rebrightening events is related to the accretion process and probably the companion star, and is independent of the nature of the compact object.

Reflares are common in many subclasses of DNe systems; either observed as well-separated rebrightenings after the end of the primary outburst (e.g., V585 Kyr; Kato & Osaki 2013), or during the decline from the peak of the main outburst caused by a reflection of the cooling wave that propagates from the outer disk edge (Dubus et al. 2001; Hameury & Lasota 2021). RZ LMi-type DNe show fast rebrightenings with very short supercycles (∼20 days; Osaki 1995). These short recurrence times are morphologically similar to the mini outbursts observed in BHXBs (Hameury et al. 2000; Zhang et al. 2019). WZ Sge systems, which are an extreme subclass of SU UMa-type DNe, exhibit much rarer superoutbursts (i.e., very long supercycle times), and are followed by rebrightenings (or reflares) as they return to quiescence (Kato 2015). Hameury & Lasota (2021) successfully explained the reflares observed in these WZ Sge systems (on the basis of the optical light curve of TCP J21040470+4631129) using the disk instability model (DIM; e.g., Lasota 2001).

In the framework of DIM, outbursts are thought to be triggered when matter accumulates in the accretion disk during quiescence, thereby heating up the disk and causing the hydrogen in the disk to ionize. This gives rises to a thermal-viscous instability, which initiates the outburst. The DIM predicts the accretion disk to have a minimum amount of matter left at the end of an outburst, and hence cannot easily explain rebrightening events, because they require a large amount of matter to be left in the disk after an outburst (e.g., Patruno et al. 2016), except under specific conditions (e.g., Zhang et al. 2019). Several other models have been used to explain the mini outbursts and/or reflares in various compact sources. For example:

1. The DIM with specific conditions, such as the presence of a hot inner disk at the end of the initial outburst (e.g., Zhang et al. 2019);
2. The mass reservoir model, as long as the effective viscosity of the disk remains large through the entire sequence of reflares (Osaki et al. 2001);
3. Irradiation of the companion star causing enhanced mass transfer through X-ray heating (e.g., Hameury et al. 2000);
4. A smaller discrete accretion event (e.g., Sturner & Shrade 2005);
5. A small-scale outburst generated by either disk instability or a change in the disk density (Patruno 2016);
6. Enhanced viscosity caused when the outer part of the disk gets irradiated and the generated mass front propagates inward (e.g., Shahbaz et al. 1998);
7. Jet brightening during hard-state decay (e.g., Jain et al. 2001; Saikia et al. 2019);
8. Activation/deactivation of the propeller effect changing the mass accretion rate due to the rapidly rotating NS magnetosphere (Hartman et al. 2011; Patruno 2016).

4.1. Comparison with Reflares in Other LMXBs

We compile a list of all BHXB sources (see Table 3) where significant rebrightening was observed within one year of the last detection of the initial outburst (either after it reached quiescence or after a gap where it is uncertain if it reached quiescence). We do not include recurrent transients (e.g., GX 339-4; Tetarenko et al. 2016) and multipeak outbursts (e.g., GRO J1655-40; Chen et al. 1997). Along with BHXBs (e.g., MAXI J1535–571 and V404Cyg; Parikh et al. 2019; Muñoz-Darias et al. 2017; Cuneo et al. 2020), such rebrightening events (at different timescales) after the main outburst are also seen in NSXBs (e.g., IGR J00291+5934; Lewis et al. 2010), as well as WZ Sge-type DNe (see, e.g., Kato 2015). We use the observation-based labeling scheme explained in Zhang et al. (2019) to classify the different rebrightening phenomena in this sample, in which a rebrightening is termed as a "reflare" if the flux did not reach quiescence before the rise in amplitude. If the flux reaches quiescence before the rebrightening, we term it a "mini outburst," provided that the flux ratio between the rebrightening peak and the primary outburst peak is less than 0.7, and the time separating the start of the quiescent period from the start of the rebrightening is less than the duration of the main outburst. On the other hand, if the duration of the main outburst is shorter, or if the flux ratio between the peak of the rebrightening and the peak of the primary outburst is more than 0.7, we term it as a "new outburst" (Zhang et al. 2019).

As discussed in Section 3.1, the 2013 rebrightenings observed in J1910.2 are reflares, and not mini outbursts. We find that it is one of the very few systems to display such unusually extreme flaring (with more than seven optical reflares). In most cases, the number of reflares or mini outbursts seen during the period of rebrightening is fewer than five. The only other BHXBs displaying more than five reflares within one year of their outbursts are XTE J1650–500 (Tomsick et al. 2003, 2004), MAXI J1535–571 (Parikh et al. 2019; Cuneo et al. 2020), and V404 Cyg (Muñoz-Darias et al. 2017; Kajava et al. 2018).

In MAXI J1535–571, at least four reflaring events were seen after the first outburst, all having an approximately constant interval between reflares of ∼31–32 days (Cuneo et al. 2020). However, unlike MAXI J1535–571, where a progressive faintness of the reflares is observed, likely due to an emptying reservoir of mass available for accretion (Parikh et al. 2019), the peak magnitude of the 2013 reflares in J1910.2 stayed almost constant. The MAXI J1535–571 reflares also exhibited state transitions and the hysteresis pattern in the HID, which is generally observed only in the main outbursts of LMXBs (except for the mini outbursts in GRS 1739–278; Yan & Yu 2017). Such a comparison is not possible for J1910.2, as there is only one X-ray detection and a few upper limits

Table 3
Sample of LMXB Outbursts with Rebrightenings within One Year of the Last Detection of the Initial Outburst

Source	BH/NS[a]	Year[b]	Classification[c]	$t_{\rm flaring}$ (d)[d]	$N_{\rm flares}$[e]	Band[f]	$\Delta t_{\rm peaks}$[g]	State[h]	References[i]
A 0620–00	BH	1975	mini outburst	∼60	1	optical	⋯	⋯	1
GRO J0422+32	BH	1992	mini outbursts	>271	2	optical	∼113	⋯	2
GRS 1716−249	BH	1993	reflares	>400	5	X-ray	50–90	hard	3
XTE J1859+226	BH	1999	mini outbursts?	∼75	3	optical	20–30	hard	4
XTE J1650–500	BH	2001	reflares?	>150	⩾7	X-ray	14.2	hard	5, 6
Swift J1753.5–0127	BH	2005	mini outburst	>151	1	both	⋯	hard	7
IGR J00291+5934	NS	2008	new outburst	>49.0	1	both	⋯	hard	8
XTE J1752–223	BH	2010	reflare?	⋯	1	both	⋯	hard	9
MAXI J1659–152	BH	2010	mini outburst	89 ± 15	1	both	⋯	hard	10, 11
MAXI J1836–194	BH	2011	reflare?	∼75	1	both	⋯	hard	12, 13
Swift J1910.2–0546	BH	2012	reflares	>245.8	⩾7	optical	42–49	hard	14, 15
GRS 1739–278	BH	2014	mini outbursts	>150	3	X-ray	∼62	hard, soft	16
V404 Cyg	BH	2015	reflares	>33	>10	both	<1	hard	17, 18
MAXI J1535–571	BH	2017	reflares	>165	⩾5	X-ray	31 − 32	hard, soft	19, 20
MAXI J1820+070	BH	2018	mini outbursts	>474	3	both	∼177	hard	21–28
MAXI J1348–630	BH	2019	mini outbursts	∼280	⩾3	both	∼90	hard	29–34
4U 1543–47	BH	2022	mini outburst, reflares	>240	⩾5	both	20–30	hard, soft	35–37

Notes.
[a] BH = black hole; NS = neutron star.
[b] Year of initial outburst.
[c] Rebrightening classification based on Zhang et al. (2019).
[d] Total duration of rebrightening interval after the initial outburst.
[e] Number of reflares during the rebrightening interval.
[f] Wave band(s) of the reported rebrightening(s) (optical, X-ray, or both).
[g] Reflare recurrence times (when >1 flare recorded).
[h] Rebrightening X-ray state (if known).
[i] **References:** (1) Charles (1998); (2) Callanan et al. (1995); (3) Hjellming et al. (1996); (4) Zurita et al. (2002); (5) Tomsick et al. (2003); (6) Tomsick et al. (2004); (7) Zhang et al. (2019); (8) Lewis et al. (2010); (9) Corral-Santana et al. (2010a); (10) Homan et al. (2013); (11) Corral-Santana et al. (2018); (12) Yang et al. (2012); (13) Krimm et al. (2012b); (14) this paper; (15) Tomsick et al. (2013); (16) Yan & Yu (2017); (17) Muñoz-Darias et al. (2017); (18) Kajava et al. (2018); (19) Parikh et al. (2019); (20) Cuneo et al. (2020); (21) Ulowetz et al. (2019); (22) Bahramian et al. (2019); (23) Baglio et al. (2019); (24) Hambsch et al. (2019); (25) Xu et al. (2019); (26) Adachi et al. (2020); (27) Sasaki et al. (2020); (28) Shaw et al. (2021) (29) Al Yazeedi et al. (2019); (30) Pirbhoy et al. (2020); (31) Shimomukai et al. (2020); (32) Zhang et al. (2020); (33) Baglio et al. (2020a); (34) Carotenuto et al. (2021); (35) Alnaqbi et al. (2022); (36) Wang et al. (2022); (37) Negoro et al. (2022).

available from Swift/XRT during the reflaring behavior. The single X-ray detection is as hard as the 2012 outburst hard-state decay, so at least for one date during the reflares we can confirm that the source was in the hard state. Moreover, as transitions are usually at higher luminosities, and these reflares are barely detected by Swift/XRT, we argue that all the reflares are probably happening in the hard state. We note that the reflares hysteresis loops observed in MAXI J1535–571 occurred at almost 100 times lower luminosities than the peak of the main outburst, with the state transitions occurring at a luminosity of $L_X \leqslant 7 \times 10^{36}\,{\rm erg\,s^{-1}}$ (which is the lowest luminosity at which hard-to-soft transitions have been observed in a BHXB; see Cuneo et al. 2020). However the only X-ray detection of J1910.2 available during the reflares is more than 1000 times lower than the outburst peak, suggesting that the 2013 reflares of J1910.2 happened in the hard state.

4.2. Origin of the 2013 Reflares

One important observation from the CMD of J1910.2 (see Section 3.5) is that it repeatedly crosses the temperature needed to ionize/neutralize the hydrogen present in the accretion disk during the rebrightening events. Typically at the end of the outburst, the temperature in the outer disk decreases, causing the hydrogen in the disk to recombine, and this sends a cooling wave that propagates inwards (Dubus et al. 2001; Lasota 2001). It eventually reaches matter in the inner disk that is so hot it cannot be cooled lower than the recombination temperature, so the cooling wave halts. At the radius where the surface density behind the cooling front becomes high enough, the disk becomes thermally unstable, initiating a new heating front to propagate outwards (Dubus et al. 2001). The CMD of J1910.2 suggests that the repeated 2013 reflares are probably due to the back-and-forth propagation of cooling and heating waves in the disk.

If the instability causing the reflares is originating at the inner disk and then propagating outwards, then the rise time of the repeated reflares, which estimates the propagation time of the heating front, suggests a viscous timescale of ∼6 days. A viscous timescale of ∼6 days is also measured from the dip in intensity seen during the 2012 outburst, provided it is also caused by a reduction in mass transfer into the inner disk (Degenaar et al. 2014; Saikia et al. 2023). A measurement of the disk viscosity parameters from the observed light-curve profile (as done using a hierarchical Bayesian approach with Markov Chain Monte Carlo fitting after removing flares in Tetarenko et al. 2018) is difficult in this case due to the lack of good coverage during the decay of the reflares. However, overall the general structure of the reflares follow a pattern of rapid heating and a relatively slower fading, similar to what is observed during main outbursts.

Numerical simulations of the DIM automatically predict reflares which are spontaneously created through repeated heating/cooling waves that cyclically ionize and recombine in the accretion disk, although the numerically produced light curves do not generally resemble those observed (Dubus et al. 2001;

Meyer & Meyer-Hofmeister 2015; Hameury & Lasota 2021). Moreover, the reflares predicted by the DIM require the density of matter to be depleted with each subsequent reflare, and hence a progressive faintness in amplitude is expected (Dubus et al. 2001); which is not observed in the case of J1910.2. However, we speculate that a heated-up companion can continuously dump matter in the disk, due to its expansion from being heated by the X-rays of the 2012 outburst. This enhanced mass transfer from the companion (in addition to the steady accretion from the companion that happens all the time) can result in an almost constant amplitude during the reflares. Another possibility is that the X-ray and optical emission show different things. X-rays trace the mass accretion rate close to the BH, and a decreasing trend of peak X-ray luminosities is expected (as seen in the X-ray light curves of MAXI J1535–571 reflares; Cuneo et al. 2020). However, the constant peak optical magnitude could correspond to the position in the CMD where the disk reaches above the H ionization temperature. From the CMDs of J1910.2 (see Figure 7), we find that the data follow the disk model very well, suggesting that the emitting area is roughly constant during the reflares. Hence it is possible that we are probing different mechanisms in both wavelengths: we could be looking at constant-area blackbody heating and cooling in the optical, while tracing the mass accretion rate in X-rays. This could be another reason why we do not have a decreasing trend of peak optical fluxes, as also seen in the optical light curves of GRO J0422+32 reflares by Callanan et al. (1995).

Overall, it is not completely clear if the reflares are caused by the same hydrogen ionization instability which triggers the main outburst or they have a different origin mechanism. However, from the changes in temperature observed during the reflares (which repeatedly cross the H ionization temperature), we consider the back-and-forth propagation of heating/cooling waves to be the most likely explanation for the 2013 reflares.

4.3. Origin of the 2014 Mini Outburst

Large-amplitude optical oscillations or violent reflares seen on shorter timescales (on timescales of hours) in sources like V404 Cyg are expected in long-period systems. The disk in such systems is much larger, and the surface densities in the outer disk will be too low to have sustained mass accretion in the inner disk, which is required for longer-timescale reflares (Kimura et al. 2016). In fact, the longer-timescale 2014 mini outburst as seen in J1910.2 is expected to be more common in BHXB systems with shorter orbital periods (<7 hr). In such short-period systems, it is speculated that the outer disk has a high enough temperature for the heating front to remain hot, thereby triggering a mini outburst (Zhang et al. 2019). Due to the lack of any deep soft X-ray observation during the outburst fade, or before this 2014 mini outburst, we do not have direct confirmation for the presence of a hot inner disk. However, recent optical fast photometry of J1910.2 indeed suggests an orbital period of <7.4 hr (Saikia et al. 2023). Previously, Casares et al. (2012) had reported an orbital period >6.2 hr from their spectroscopic study, assuming that the velocity changes in Hα emission are cause by binary motion. Later, a fairly short orbital period (∼2–4 hr) was proposed based on the small size of its disk with a radius of $\sim 4 \times 10^9$ cm (Degenaar et al. 2014) and its variable optical emission (Lloyd et al. 2012). Such a short orbital period can ensure the presence of a hot inner disk at the end of the outburst decay, which could have triggered the mini outburst seen in J1910.2.

5. Summary and Conclusions

In this work, we present long-term optical monitoring of the candidate BH transient X-ray binary Swift J1910.2–0546 from 2012 to 2022 using the Faulkes Telescopes and LCO. We report two periods of rebrightening activities previously undocumented in the literature, which include a series of at least seven quasi-periodic, high-amplitude (∼3 mag) optical reflares in 2013, and a mini outburst with two peaks in 2014. We find that the source shows a bluer-when-brighter behavior during both of the rebrightening episodes in 2013 and 2014. The optical colors during these epochs are consistent with blackbody heating and cooling between 4500 and 9500 K, suggesting that the flares could be caused by repetitive heating and cooling waves traveling through the accretion disk. We compare them with rebrightening events observed in other BHXBs within one year of an outburst, and show that the repeated reflaring behavior of J1910.2 is highly unusual among BHXBs. We discuss the different scenarios which could cause such extreme flaring, and propose that they arise from a sequence of heating and cooling front reflections in the accretion disk following the DIM, probably due to the presence of a hot inner disk at the end of the 2012 outburst.

D.M.R. and D.M.B. acknowledge the support of the NYU Abu Dhabi Research Enhancement Fund under grant RE124. This work uses data from the Faulkes Telescope Project, which is an education partner of Las Cumbres Observatory (LCO). The Faulkes Telescopes are maintained and operated by LCO. This work also makes use of data supplied by the UK Swift Science Data Centre at the University of Leicester, and the MAXI data provided by RIKEN, JAXA, and the MAXI team.

Appendix

Table A1–A4 provides the optical magnitudes of Swift J1910.2 obtained with the Faulkes/LCO telescopes during the long-term monitoring of 2012-2022 in four different filters (i′, B, V and R, respectively). Table A5 provides the UV magnitudes and X-ray count-rates of the observations performed with Swift during the 2013-2014 re-brightening period.

Table A1
Faulkes/LCO i' Detections of J1910.2 between 2012 June and 2022 March

MJD	Mag	Error	MJD	Mag	Error	MJD	Mag	Error
56103.57914	15.411	0.004	56838.35656	20.853	0.120	58588.77569	21.039	0.076
56113.54654	15.744	0.009	56845.50696	19.985	0.132	58590.51219	20.771	0.113
56121.43063	15.646	0.003	56853.52194	18.926	0.210	58617.53223	21.283	0.060
56124.71013	15.720	0.003	56862.51814	20.256	0.071	58639.53935	20.934	0.117
56132.55873	15.780	0.003	56866.51205	20.681	0.091	58661.61785	21.649	0.157
56136.46433	15.747	0.003	56874.32180	17.299	0.005	58668.59015	20.934	0.061
56140.51726	15.889	0.011	56880.55142	17.790	0.034	58683.35748	21.223	0.103
56145.50797	15.857	0.003	56887.36128	18.235	0.009	58688.49973	21.435	0.067
56145.52121	15.853	0.003	56894.31195	18.615	0.009	58696.59538	20.829	0.064
56152.54340	15.999	0.003	56980.19925	20.800	0.119	58703.30254	21.426	0.064
56157.30921	16.086	0.004	56985.20147	20.884	0.101	58709.63468	21.036	0.179
56159.47125	16.126	0.006	57076.65770	20.791	0.109	58720.49434	21.425	0.065
56165.39475	16.507	0.009	57084.63471	21.047	0.201	58730.45624	21.164	0.076
56168.43164	16.805	0.138	57103.58997	20.613	0.088	58733.38005	21.261	0.139
56173.41654	16.309	0.003	57113.63768	21.111	0.138	58737.48772	21.405	0.165
56180.51398	16.119	0.003	57121.58267	21.056	0.203	58745.32408	21.555	0.084
56187.39273	16.214	0.005	57132.60743	20.961	0.092	58765.31194	21.497	0.161
56188.42123	16.234	0.004	57139.74993	19.669	0.060	58772.30862	21.097	0.102
56195.40349	16.227	0.009	57148.51690	21.004	0.177	58774.44523	21.368	0.084
56199.28902	16.289	0.005	57160.53437	21.230	0.118	58813.19642	21.056	0.130
56201.30782	16.276	0.005	57167.47057	20.943	0.086	58908.78342	21.232	0.175
56201.48097	16.315	0.005	57181.57528	21.163	0.147	58928.76823	20.989	0.087
56208.42422	16.428	0.004	57195.50714	21.768	0.112	58939.77835	20.953	0.078
56208.42725	16.444	0.005	57202.46687	21.720	0.201	58945.70879	20.856	0.194
56213.43197	16.360	0.004	57209.43227	21.385	0.216	58951.73146	21.369	0.229
56216.23302	16.451	0.006	57230.33313	21.126	0.183	58960.75695	21.197	0.098
56220.40988	16.437	0.006	57237.39146	21.377	0.140	58966.49496	20.840	0.064
56229.29271	16.169	0.011	57244.32026	21.268	0.079	58971.55310	21.281	0.076
56235.42001	15.598	0.003	57305.29322	21.387	0.163	58985.61396	20.859	0.089
56370.63724	17.124	0.009	57319.26439	21.209	0.238	59015.48351	21.615	0.066
56388.59126	19.154	0.073	57449.63776	17.964	0.027	59019.57914	21.108	0.033
56389.71272	19.214	0.032	57482.62775	21.249	0.159	59027.39162	20.890	0.010
56411.49206	17.289	0.044	57538.57450	21.588	0.173	59031.53659	21.292	0.026
56432.77561	19.464	0.093	57552.60284	21.297	0.216	59042.55843	21.294	0.015
56438.77293	19.913	0.218	57575.47110	21.300	0.148	59049.38921	21.122	0.055
56444.49491	19.386	0.058	57582.34497	21.522	0.227	59070.46009	21.069	0.076
56446.67371	18.891	0.025	57604.40432	20.742	0.214	59079.36069	21.444	0.063
56451.36716	17.339	0.015	57636.43600	21.091	0.145	59098.40355	21.246	0.103
56451.70871	17.373	0.008	57636.57138	21.025	0.213	59105.36726	21.660	0.077
56459.36371	17.633	0.018	57650.33851	21.297	0.230	59137.47372	21.096	0.099
56459.56645	17.558	0.009	57662.25502	21.733	0.248	59164.40070	20.982	0.192
56465.61520	17.461	0.015	57668.41487	20.132	0.177	59326.69727	21.074	0.079
56472.44247	18.108	0.035	57681.41133	21.066	0.197	59328.64053	21.063	0.148
56475.72691	18.323	0.018	57693.23105	20.161	0.151	59336.77785	21.435	0.140
56479.62546	19.221	0.038	57879.59531	21.730	0.233	59352.69291	21.098	0.060
56487.32529	19.311	0.051	57898.78906	20.807	0.210	59357.55632	20.917	0.119
56493.57297	17.180	0.014	57959.51273	20.899	0.174	59401.62041	21.282	0.076
56494.32294	17.436	0.073	58271.41535	20.776	0.232	59454.48904	21.417	0.084
56502.55416	17.941	0.075	58274.61550	21.018	0.162	59459.47716	21.126	0.087
56507.35435	17.727	0.017	58282.55969	21.081	0.074	59492.44737	21.195	0.081
56508.49108	17.609	0.009	58290.68478	21.007	0.086	59505.46457	20.690	0.106
56514.49400	18.031	0.012	58297.54633	19.028	0.122	59514.43583	21.050	0.141
56516.45863	18.289	0.028	58303.42136	21.748	0.116	59518.43300	21.171	0.147
56521.48976	19.479	0.103	58309.56344	21.006	0.086	59623.27219	16.462	0.011
56528.43259	18.542	0.019	58316.50208	21.012	0.069	59623.28173	16.501	0.021
56535.28511	19.659	0.079	58337.49055	21.235	0.093	59624.28401	16.676	0.022
56535.40493	19.640	0.109	58344.50426	21.206	0.078	59625.28332	16.729	0.031
56536.42724	19.072	0.030	58358.48956	21.455	0.134	59625.50953	16.861	0.032
56542.41646	17.061	0.006	58366.51429	21.241	0.180	59625.50966	16.791	0.020
56556.33697	18.384	0.049	58372.50783	20.895	0.108	59628.39353	17.073	0.046
56564.52723	19.750	0.052	58388.39902	21.258	0.084	59628.50150	17.025	0.024
56567.39740	18.798	0.023	58399.48422	20.754	0.075	59629.25470	17.127	0.028
56571.44275	18.018	0.016	58412.39558	21.064	0.146	59629.39078	17.105	0.030
56573.27960	18.213	0.063	58417.27583	21.314	0.201	59630.38800	17.189	0.029

Table A1
(Continued)

MJD	Mag	Error	MJD	Mag	Error	MJD	Mag	Error
56579.26550	19.091	0.119	58442.21064	21.465	0.194	59632.12909	17.275	0.034
56587.25545	18.638	0.044	58552.61741	21.139	0.186	59633.12638	17.410	0.040
56587.42513	18.646	0.028	58561.59803	21.112	0.112	59633.38451	17.448	0.039
56599.42466	17.502	0.014	58563.58575	21.279	0.204	59634.39863	17.510	0.057
56733.62663	19.891	0.086	58572.64391	20.978	0.074	59637.14371	17.679	0.097
56819.56681	20.656	0.167	58582.53598	20.890	0.104	59658.76599	20.696	0.144
56834.61483	20.953	0.182						

Table A2
Faulkes/LCO *B* Detections of J1910.2 between 2012 June and 2013 July

MJD	Mag	Error	MJD	Mag	Error	MJD	Mag	Error
56124.44045	16.668	0.006	56127.44392	16.876	0.006	56132.40759	16.916	0.006
56124.44823	16.674	0.006	56127.44621	16.859	0.006	56132.40994	16.907	0.006
56124.45531	16.693	0.006	56127.44847	16.892	0.006	56132.41232	16.922	0.006
56124.48141	16.811	0.006	56127.45085	16.884	0.006	56132.41882	16.900	0.006
56124.49092	16.808	0.006	56127.45325	16.867	0.006	56132.42124	16.912	0.006
56124.49324	16.806	0.006	56127.45551	16.846	0.006	56132.42364	16.912	0.006
56124.49565	16.805	0.006	56127.46098	16.854	0.006	56132.42621	16.912	0.006
56124.49800	16.798	0.006	56127.46348	16.864	0.006	56132.42863	16.913	0.006
56124.50043	16.797	0.006	56127.46592	16.841	0.006	56132.43106	16.906	0.006
56124.50278	16.789	0.006	56127.47746	16.835	0.006	56132.43346	16.905	0.006
56124.50514	16.793	0.005	56127.47981	16.885	0.006	56132.43897	16.902	0.006
56124.50749	16.787	0.005	56127.48214	16.853	0.006	56132.44130	16.906	0.006
56124.50984	16.792	0.006	56127.48443	16.883	0.006	56132.44368	16.892	0.006
56124.51228	16.777	0.005	56127.48670	16.880	0.006	56132.44611	16.897	0.006
56124.51469	16.783	0.006	56127.48896	16.873	0.006	56132.44844	16.906	0.006
56124.51704	16.784	0.005	56127.49123	16.872	0.006	56132.45077	16.922	0.006
56124.54456	16.810	0.006	56127.50781	16.903	0.006	56132.45307	16.919	0.006
56124.54704	16.815	0.006	56127.51200	16.904	0.006	56132.45542	16.907	0.006
56124.54955	16.816	0.006	56127.52455	16.904	0.006	56132.45772	16.919	0.006
56124.55217	16.827	0.006	56127.52687	16.943	0.007	56132.46000	16.916	0.006
56124.55450	16.815	0.006	56127.52925	16.912	0.007	56132.46227	16.909	0.006
56124.55685	16.834	0.006	56127.53152	16.910	0.007	56132.46456	16.915	0.006
56124.55934	16.818	0.006	56127.53432	16.925	0.007	56132.46691	16.912	0.006
56124.69002	16.826	0.006	56127.53660	16.898	0.007	56132.46921	16.906	0.006
56124.69234	16.815	0.007	56127.53889	16.915	0.007	56132.47157	16.914	0.006
56124.69463	16.810	0.006	56127.54383	16.905	0.007	56132.47398	16.919	0.006
56124.69695	16.813	0.006	56127.54615	16.923	0.007	56132.47638	16.924	0.006
56124.69925	16.804	0.006	56127.54850	16.905	0.007	56132.48105	16.906	0.006
56124.70154	16.799	0.006	56127.55318	16.901	0.007	56132.48338	16.916	0.006
56124.70382	16.787	0.006	56127.55544	16.912	0.007	56132.48886	16.926	0.009
56127.41841	16.879	0.006	56127.55778	16.911	0.007	56132.49120	16.912	0.009
56127.42086	16.890	0.006	56132.38015	16.942	0.008	56132.49352	16.892	0.014
56127.42324	16.881	0.006	56132.38258	16.922	0.008	56132.49663	16.923	0.007
56127.42554	16.896	0.006	56132.38506	16.932	0.008	56173.44007	17.502	0.010
56127.42782	16.890	0.006	56132.38771	16.929	0.007	56173.44645	17.456	0.010
56127.43019	16.899	0.006	56132.39003	16.931	0.008	56173.45258	17.464	0.011
56127.43250	16.872	0.006	56132.39283	16.925	0.007	56173.45839	17.468	0.016
56127.43482	16.899	0.006	56132.39812	16.906	0.007	56173.46677	17.465	0.011
56127.43712	16.895	0.006	56132.40048	16.902	0.007	56180.44806	17.163	0.011
56127.43938	16.888	0.006	56132.40285	16.918	0.007	56180.45017	17.153	0.007
56127.44164	16.906	0.006	56132.40528	16.903	0.006	56474.49156	19.715	0.025

Table A3
Faulkes/LCO *V* Detections of J1910.2 between 2012 June and 2014 August

MJD	Mag	Error	MJD	Mag	Error	MJD	Mag	Error
56103.58068	15.714	0.005	56194.46125	16.494	0.015	56446.67526	19.882	0.045
56113.54809	16.068	0.024	56194.46316	16.523	0.021	56451.36870	17.705	0.030
56121.43220	15.929	0.004	56194.46455	16.527	0.022	56451.71034	17.732	0.010
56124.44263	16.001	0.006	56194.46594	16.526	0.023	56459.56807	18.067	0.014
56124.45018	16.019	0.005	56194.47004	16.549	0.022	56465.61683	17.997	0.028
56124.48372	16.060	0.005	56194.47140	16.553	0.021	56479.62706	20.383	0.084
56124.51887	16.041	0.007	56194.47274	16.546	0.020	56493.57457	17.526	0.020
56124.70598	16.035	0.004	56194.47541	16.547	0.021	56508.49263	18.067	0.013
56124.71167	16.042	0.005	56194.47673	16.527	0.020	56514.49555	18.610	0.018
56127.51397	16.067	0.004	56195.40506	16.528	0.016	56528.43416	19.262	0.032
56132.48663	16.135	0.013	56201.30941	16.578	0.010	56535.28670	20.292	0.230
56132.56032	16.144	0.005	56201.48257	16.615	0.012	56536.42883	19.809	0.050
56140.51880	16.289	0.024	56208.42884	16.753	0.008	56542.41800	17.444	0.008
56145.50952	16.243	0.005	56209.44072	16.699	0.007	56564.52880	20.818	0.150
56145.52276	16.259	0.005	56209.44278	16.706	0.007	56567.39895	19.509	0.035
56152.54500	16.417	0.005	56213.43352	16.715	0.006	56571.44429	18.573	0.024
56157.31075	16.478	0.006	56216.23456	16.778	0.009	56587.25700	19.410	0.115
56165.39635	16.914	0.018	56220.41149	16.827	0.012	56599.42624	17.815	0.013
56173.41813	16.677	0.006	56235.42155	16.321	0.006	56810.51529	21.632	0.129
56180.41980	16.330	0.005	56388.59280	19.514	0.135	56866.50853	21.613	0.224
56180.42203	16.342	0.005	56389.71427	20.359	0.120	56874.31833	17.635	0.008
56180.44584	16.375	0.007	56389.71427	20.359	0.120	56880.54816	18.208	0.067
56180.51562	16.466	0.006	56411.49360	17.673	0.093	56887.35765	18.737	0.013
56194.45347	16.576	0.015	56443.43916	19.905	0.231	56894.30856	19.212	0.016
56194.45593	16.523	0.020	56443.44273	20.528	0.197			

Table A4
Faulkes/LCO *R* Detections of J1910.2 between 2012 June and 2014 August

MJD	Mag	Error	MJD	Mag	Error	MJD	Mag	Error
56092.63578	15.155	0.004	56201.31089	16.260	0.006	56494.32599	17.223	0.088
56092.63734	15.158	0.004	56201.48405	16.313	0.006	56502.55729	18.037	0.019
56092.63872	15.157	0.011	56208.43036	16.426	0.006	56507.35740	17.814	0.020
56092.64142	15.145	0.013	56213.43500	16.354	0.004	56508.49416	17.675	0.009
56092.64278	15.132	0.012	56216.23606	16.426	0.006	56514.49704	18.128	0.012
56103.58217	15.376	0.003	56220.41298	16.455	0.006	56516.46172	18.463	0.037
56113.54955	15.766	0.012	56229.29576	16.218	0.017	56521.49279	19.628	0.117
56121.43366	15.588	0.003	56235.42303	15.873	0.003	56528.43565	18.702	0.020
56124.48536	15.727	0.004	56353.62190	19.258	0.210	56535.40799	19.749	0.120
56124.71312	15.706	0.003	56370.64035	17.217	0.011	56536.43031	19.178	0.029
56127.51599	15.750	0.002	56388.59428	19.217	0.080	56542.41950	17.065	0.006
56127.56545	15.755	0.003	56389.71573	19.446	0.036	56556.33999	18.532	0.076
56127.56845	15.758	0.003	56411.49513	17.446	0.066	56564.53026	19.912	0.065
56127.57133	15.759	0.003	56432.77876	19.660	0.106	56567.40041	18.927	0.023
56132.56180	15.791	0.003	56438.77597	19.833	0.194	56571.44575	18.032	0.015
56136.46744	15.742	0.004	56444.49797	19.796	0.098	56587.25851	19.048	0.072
56140.52028	15.918	0.013	56446.67672	19.073	0.025	56587.42817	18.884	0.030
56145.52425	15.885	0.003	56451.37023	17.377	0.018	56599.42778	17.463	0.010
56152.54653	16.010	0.003	56451.71187	17.346	0.007	56810.51699	20.939	0.065
56157.31226	16.114	0.004	56459.36687	17.724	0.021	56813.40803	20.549	0.205
56159.47428	16.150	0.013	56459.56959	17.640	0.010	56826.61435	21.211	0.202
56165.39784	16.563	0.011	56465.61830	17.570	0.018	56838.35485	21.689	0.237
56168.43468	17.217	0.097	56472.44550	17.983	0.028	56862.51641	21.156	0.124
56173.41964	16.314	0.004	56475.72997	18.489	0.024	56866.51022	21.114	0.141
56180.51710	16.123	0.003	56479.62853	19.439	0.039	56874.32000	17.282	0.005
56187.39581	16.190	0.006	56481.37116	20.288	0.224	56880.54973	17.863	0.042
56188.42426	16.211	0.004	56487.32839	19.939	0.092	56887.35942	18.289	0.009
56195.40656	16.186	0.009	56493.57606	17.166	0.013	56894.31018	18.754	0.011
56199.29213	16.265	0.006						

Table A5
Swift UVOT and XRT (2–10 keV) Observations of Swift J1910.2–0546 During the 2013–2014 Rebrightening Period

MJD	UVOT Filter	Mag	2–10 keV Count Rate
56360.4491	*U*	19.52 ± 0.1	<0.004
56422.6641	*uvm2*	>21.28	0.05 ± 0.01
56426.9808	*uvm2*	>21.58	<0.006
56438.0399	*uw1*	>21.25	<0.009
56560.9132	*B*	>18.51	<0.004
	uvm2	>20.50	
	U	>19.19	
	V	>17.76	
	uw1	>19.87	
	uw2	>20.97	

ORCID iDs

Payaswini Saikia https://orcid.org/0000-0002-5319-6620
David M. Russell https://orcid.org/0000-0002-3500-631X
M. C. Baglio https://orcid.org/0000-0003-1285-4057
D. M. Bramich https://orcid.org/0000-0002-1583-6519
Kevin Alabarta https://orcid.org/0000-0003-0168-9906
Fraser Lewis https://orcid.org/0000-0003-3352-2334

References

Adachi, R., Murata, K. L., Oeda, M., et al. 2020, ATel, 13502, 1
Al Yazeedi, A., Russell, D. M., Lewis, F., et al. 2019, ATel, 13188, 1
Alnaqbi, J., Saikia, P., Casella, P., et al. 2022, ATel, 15254, 1
Baglio, M. C., Russell, D. M., Bramich, D. M., et al. 2020a, ATel, 13710, 1
Baglio, M. C., Russell, D. M., Crespi, S., et al. 2020b, ApJ, 905, 87
Baglio, M. C., Russell, D. M., Qaissieh, T. A., et al. 2019, ATel, 12596, 1
Baglio, M. C., Saikia, P., Russell, D. M., et al. 2022, ApJ, 930, 20
Bahramian, A., Motta, S., Atri, P., & Miller-Jones, J. 2019, ATel, 12573, 1
Bellm, E. C., Kulkarni, S. R., Graham, M. J., et al. 2019, PASP, 131, 018002
Blandford, R. D., & Königl, A. 1979, ApJ, 232, 34
Brown, T. M., Baliber, N., Bianco, F. B., et al. 2013, PASP, 125, 1031
Burrows, D. N., Hill, J. E., Nousek, J. A., et al. 2005, SSRv, 120, 165
Buxton, M. M., Bailyn, C. D., Capelo, H. L., et al. 2012, AJ, 143, 130
Callanan, P. J., Garcia, M. R., McClintock, J. E., et al. 1995, ApJ, 441, 786
Cardelli, J. A., Clayton, G. C., & Mathis, J. S. 1989, ApJ, 345, 245
Carotenuto, F., Corbel, S., Tremou, E., et al. 2021, MNRAS, 504, 444
Casares, J., Rodriguez-Gil, P., Zurita, C., et al. 2012, ATel, 4347, 1
Charles, P., Cornelisse, R., & Casares, J. 2012, ATel, 4210, 1
Charles, P. A. 1998, in ASP Conf. Ser. 137, Wild Stars in the Old West, ed. S. Howell, E. Kuulkers, & C. Woodward (San Francisco, CA: ASP), 220
Chen, W., Shrader, C. R., & Livio, M. 1997, ApJ, 491, 312
Corbel, S., Fender, R. P., Tzioumis, A. K., et al. 2000, A&A, 359, 251
Corral-Santana, J. M., Casares, J., & Rodríguez-Gil, P. 2010a, ATel, 2805, 1
Corral-Santana, J. M., Rodríguez-Gil, P., Hurley, D., & Casares, J. 2010b, ATel, 2845, 1
Corral-Santana, J. M., Torres, M. A. P., Shahbaz, T., et al. 2018, MNRAS, 475, 1036
Cuneo, V. A., Alabarta, K., Zhang, L., et al. 2020, MNRAS, 496, 1001
Degenaar, N., Maitra, D., Cackett, E. M., et al. 2014, ApJ, 784, 122
Drake, A. J., Djorgovski, S. G., Mahabal, A. A., et al. 2017, ATel, 10297, 1
Dubus, G., Hameury, J.-M., & Lasota, J.-P. 2001, A&A, 373, 251
Evans, P. A., Beardmore, A. P., Page, K. L., et al. 2007, A&A, 469, 379
Evans, P. A., Beardmore, A. P., Page, K. L., et al. 2009, MNRAS, 397, 1177
Falcke, H., Körding, E., & Markoff, S. 2004, A&A, 414, 895
Fender, R. 2004, NewAR, 48, 1399
Foight, D. R., Güver, T., Özel, F., & Slane, P. O. 2016, ApJ, 826, 66
Goodwin, A. J., Russell, D. M., Galloway, D. K., et al. 2020, MNRAS, 498, 3429
Hambsch, J., Ulowetz, J., Vanmunster, T., Cejudo, D., & Patterson, J. 2019, ATel, 13014, 1
Hameury, J.-M., & Lasota, J.-P. 2021, A&A, 650, A114
Hameury, J. M., Lasota, J. P., & Warner, B. 2000, A&A, 353, 244
Hartman, J. M., Galloway, D. K., & Chakrabarty, D. 2011, ApJ, 726, 26
Hickish, J., Razavi-Ghods, N., Perrott, Y. C., et al. 2018, MNRAS, 475, 5677
Hill, J. E., Klar, R., Cheruvu, C., et al. 2004, Proc. SPIE, 5165, 217
Hjellming, R. M., Rupen, M. P., Shrader, C. R., et al. 1996, ApJL, 470, L105
Homan, J., Fridriksson, J. K., Jonker, P. G., et al. 2013, ApJ, 775, 9
Hosokawa, R., Murata, K. L., Niwano, M., et al. 2022, ATel, 15226, 1
Hynes, R. I. 2005, ApJ, 623, 1026
Jain, R. K., Bailyn, C. D., Orosz, J. A., McClintock, J. E., & Remillard, R. A. 2001, ApJL, 554, L181
Kajava, J. J. E., Motta, S. E., Sanchez-Fernandez, C., & Kuulkers, E. 2018, A&A, 616, A129
Kalemci, E., Dincer, T., Tomsick, J. A., et al. 2013, ApJ, 779, 95
Kalemci, E., Arabacı, M. Ö., Güver, T., et al. 2014, MNRAS, 445, 1288
Kato, T. 2015, PASJ, 67, 108
Kato, T., & Osaki, Y. 2013, PASJ, 65, 97
Kimura, M., Isogai, K., Kato, T., et al. 2016, Natur, 529, 54
Koljonen, K. I. I., Russell, D. M., Corral-Santana, J. M., et al. 2016, MNRAS, 460, 942
Kong, A. K. H. 2022, ATel, 15229, 1
Krimm, H. A., Barthelmy, S. D., Baumgartner, W., et al. 2012a, ATel, 4139, 1
Krimm, H. A., Barthelmy, S. D., Baumgartner, W., et al. 2012b, ATel, 3966, 1
Lasota, J.-P. 2001, NewAR, 45, 449
Lewis, F., Russell, D. M., Fender, R. P., Roche, P., & Clark, J. S. 2008, in Proc. of the VII Microquasar Workshop: Microquasars and Beyond (Trieste: SISSA), PoS(MQW7), 069
Lewis, F., Russell, D. M., Jonker, P. G., et al. 2010, A&A, 517, A72
Lloyd, C., Oksanen, A., Starr, P., Darlington, G., & Pickard, R. 2012, ATel, 4246
López, K. M., Jonker, P. G., Torres, M. A. P., et al. 2019, MNRAS, 482, 2149
MacDonald, R. K. D., Bailyn, C. D., Buxton, M., et al. 2014, ApJ, 784, 2
Maitra, D., & Bailyn, C. D. 2008, ApJ, 688, 537
Matsuoka, M., Kawasaki, K., Ueno, S., et al. 2009, PASJ, 61, 999
Merloni, A., Heinz, S., & Di Matteo, T. 2003, MNRAS, 345, 1057
Meyer, F., & Meyer-Hofmeister, E. 2015, PASJ, 67, 52
Muñoz-Darias, T., Casares, J., Mata Sánchez, D., et al. 2017, MNRAS, 465, L124
Nakahira, S., Negoro, H., Shidatsu, M., et al. 2014, PASJ, 66, 84
Negoro, H., Nakajima, M., Urabe, S., et al. 2022, ATel, 15715, 1
Osaki, Y. 1995, PASJ, 47, L25
Osaki, Y., Meyer, F., & Meyer-Hofmeister, E. 2001, A&A, 370, 488
Parikh, A. S., Russell, T. D., Wijnands, R., et al. 2019, ApJL, 878, L28
Patruno, A. 2016, ApJ, 839, 51
Patruno, A., Maitra, D., Curran, P. A., et al. 2016, ApJ, 817, 100
Pirbhoy, S. F., Baglio, M. C., Russell, D. M., et al. 2020, ATel, 13451, 1
Roming, P. W. A., Kennedy, T. E., Mason, K. O., et al. 2005, SSRv, 120, 95
Russell, D. M., Bramich, D. M., Lewis, F., et al. 2019, AN, 340, 278
Russell, D. M., Casella, P., Kalemci, E., et al. 2020, MNRAS, 495, 182
Russell, D. M., Maitra, D., Dunn, R. J. H., & Fender, R. P. 2011, MNRAS, 416, 2311
Russell, D. M., Qasim, A. A., Bernardini, F., et al. 2018, ApJ, 852, 90
Saikia, P., Baglio, M. C., Russell, D. M., et al. 2021, ATel, 14302, 1
Saikia, P., Kording, E., Coppejans, D. L., et al. 2018, A&A, 616, A152
Saikia, P., Körding, E., & Falcke, H. 2015, MNRAS, 450, 2317
Saikia, P., Russell, D. M., Alabarta, K., et al. 2022a, ATel, 15303, 1
Saikia, P., Russell, D. M., Baglio, M. C., et al. 2022c, ApJ, 932, 38
Saikia, P., Russell, D. M., Bramich, D. M., et al. 2019, ApJ, 887, 21
Saikia, P., Russell, D. M., Pirbhoy, S. F., et al. 2023, MNRAS, submitted
Sasaki, R., Negoro, H., Nakahira, S., et al. 2020, ATel, 13530, 1
Shahbaz, T., Charles, P. A., & King, A. R. 1998, MNRAS, 301, 382
Shaw, A. W., Plotkin, R. M., Miller-Jones, J. C. A., et al. 2021, ApJ, 907, 34
Shimomukai, R., Negoro, H., Nakajima, M., et al. 2020, ATel, 13459, 1
Sturner, S. J., & Shrade, C. R. 2005, ApJ, 625, 923
Tetarenko, B. E., Lasota, J.-P., Heinke, C. O., Dubus, G., & Sivakoff, G. R. 2018, Natur, 554, 69
Tetarenko, B. E., Sivakoff, G. R., Heinke, C. O., & Gladstone, J. C. 2016, ApJS, 222, 15
Tominaga, M., Nakahira, S., Negoro, H., et al. 2022, ATel, 15214, 1
Tomsick, J. A., Corbel, S., Rodriguez, J., & Tzioumis, T. 2013, ATel, 5063, 1
Tomsick, J. A., Kalemci, E., Corbel, S., & Kaaret, P. 2003, ApJ, 592, 1100
Tomsick, J. A., Kalemci, E., & Kaaret, P. 2004, ApJ, 601, 439
Tucker, M. A., Shappee, B. J., Holoien, T. W.-S., et al. 2018, ApJL, 867, L9
Ulowetz, J., Myers, G., & Patterson, J. 2019, ATel, 12567, 1
Usui, R., Nakahira, S., Tomida, H., et al. 2012, ATel, 4140, 1
van Velzen, S., Bellm, E. C., & van Roestel, J. 2019, ATel, 12796, 1
Wang, J., Kara, E., Steiner, J. F., et al. 2022, ATel, 15253, 1
Williams, D., Motta, S., Rhodes, L., et al. 2022, ATel, 15219, 1

Wu, J., Orosz, J. A., McClintock, J. E., et al. 2016, ApJ, 825, 46
Xu, Y., Harrison, F., & Tomsick, J. 2019, ATel, 13025, 1
Yan, Z., & Yu, W. 2017, MNRAS, 470, 4298
Yang, Y. J., Wijnands, R., & Kennea, J. A. 2012, ATel, 3975, 1
Zhang, G.-B., Bernardini, F., Russell, D. M., et al. 2019, ApJ, 876, 5
Zhang, L., Altamirano, D., Remillard, R., et al. 2020, ATel, 13465, 1
Zurita, C., Sánchez-Fernández, C., Casares, J., et al. 2002, MNRAS, 334, 999
Zwart, J. T. L., Barker, R. W., Biddulph, P., et al. 2008, MNRAS, 391, 1545